Evolution of *E. coli* in a mouse model of inflammatory bowel disease leads to a disease-specific bacterial genotype and trade-offs with clinical relevance

Rahul Unni[1,2,#], Nadia Andrea Andreani[1,2,#], Marie Vallier[1,2,§,#], Silke Heinzmann[3], Jan Taubenheim[4], Martina A. Guggeis[5,6], Florian Tran[5,6], Olga Vogler[1,2], Jan-Bernd Hövener[7], Philip Rosenstiel[5], Christoph Kaleta[4], Astrid Dempfle[8], Daniel Unterweger[1,2,*], John F. Baines[1,2,*]

[1] Max Planck Institute for Evolutionary Biology, August-Thienemann-Str. 2, 24306 Plön, Germany.
[2] Section of Evolutionary Medicine, Institute for Experimental Medicine, Kiel University, Arnold-Heller-Str. 3, 24105 Kiel, Germany.
[3] Research Unit Analytical BioGeoChemistry, Helmholtz Munich, 85764 Neuherberg, Germany.
[4] Research Group Medical Systems Biology, Institute for Experimental Medicine, Kiel University, Michaelisstr. 5, 24105 Kiel, Germany.
[5] Institute of Clinical Molecular Biology, Christian-Albrechts-University Kiel and University Medical Center Schleswig-Holstein, Kiel, Germany.
[6] Department of Internal Medicine I, University Medical Center Schleswig-Holstein, Kiel, Germany.
[7] Section Biomedical Imaging, Molecular Imaging North Competence Center (MOIN CC), Department of Radiology and Neuroradiology, University Medical Center Kiel, Kiel University, Kiel, Germany.
[8] Institute of Medical Informatics and Statistics, Kiel University, Kiel, Germany
[#] These authors contributed equally
[§] Current affiliation: : Valbiotis, R&D Center, 20-22 Rue Henri et Gilberte Goudier, 63200 Riom, France
* Corresponding authors: baines@evolbio.mpg.de, unterweger@iem.uni-kiel.de

Abstract

Objective: Inflammatory bowel disease (IBD) is a persistent inflammatory condition affecting the gastrointestinal tract, presenting significant challenges in its management and treatment. Despite the knowledge that within-host bacterial evolution occurs in the intestine, the disease has so far rarely been studied from an evolutionary perspective. In this study, we aimed to investigate resident bacterial evolution during intestinal inflammation, and whether- and how disease-related bacterial genetic changes may present trade-offs with potential therapeutic importance.
Design: Here, we perform an *in vivo* evolution experiment of *E. coli* in a gnotobiotic mouse model of IBD, followed by multiomic analyses to identify disease-specific genetic and phenotypic changes in bacteria evolved in an inflamed versus non-inflamed control environment.
Results: Our results demonstrate distinct evolutionary changes in *E. coli* specific to inflammation, including a single nucleotide variant that independently reached high frequency in all inflamed mice. Using *ex vivo* fitness assays, we find that these changes are associated with a higher fitness in an inflamed environment compared to isolates derived from non-inflamed mice. Further, using large-scale phenotypic assays, we show that bacterial adaptation to inflammation results in clinically relevant phenotypes, which intriguingly include collateral sensitivity towards antibiotics.
Conclusions: Bacterial evolution in an inflamed gut yields specific genetic and phenotypic signatures. These results may serve as a basis for developing novel, evolution-informed treatment approaches for patients with intestinal inflammation.

Introduction

Dysbiosis of the intestinal microbial community, characterized by alterations in bacterial composition and function, is a hallmark of inflammatory bowel disease (IBD). The nature of these microbial imbalances has been described extensively and at numerous complementary levels, including diversity parameters, taxonomic- and functional genomic changes, as well as at the level of gene expression (1–6). This important body of work accounts for changes observed at the ecological level, while the latter also considers the potential contribution of phenotypic plasticity of gut microbes to disease susceptibility. Moreover, numerous studies have highlighted the association of dysbiotic microbial signatures with distinct clinical IBD subtypes, including Crohn's disease (CD) and ulcerative colitis (UC), further emphasizing the intricate relationship between gut microbiota and disease pathogenesis (3,4,7).

While research has focused extensively on the altered ecology of gut microbiota in IBD, its potential for evolutionary change during disease pathogenesis has received comparatively limited attention. Numerous recent studies, however, have unveiled the capacity of bacteria to undergo adaptive evolution within the host environment, including the gut [reviewed in (8)]. This phenomenon is evident in both mouse models (9–11) and human subjects (12), even in the absence of overt disease. Importantly, other recent studies indicate that evolutionary change also occurs in the context of host inflammation. Elhenawy et al. focused on the CD-related adherent-invasive *E. coli* (AIEC) using a murine model of chronic colonization, and revealed the evolution of lineages displaying enhanced invasive and metabolic capabilities (13). Notably, they found that the fitness benefits conferred by increased motility were specific to the host environment, suggesting an evolutionary trade-off. In a second study exploring bacterial evolution in aging mice, significant differences in *E. coli* evolution between old and young mice were revealed (14). The aged mouse environment exhibited increased inflammation, leading to the specific targeting of stress-related functions in *E. coli*.

The findings above emphasize the importance of including evolutionary perspectives when studying gut microbiome dysbiosis. In particular, documenting bacterial evolution within the inflamed gut carries the potential to reveal the *timing* of disease-specific signatures, i.e., may help disentangle the classical “chicken or egg” dilemma in microbiome research (15), as well as to shed light on potential trade-offs resulting from adaptive changes. Evolutionary trade-offs occur when an increase in fitness in one environment is accompanied by a decrease in fitness in another (16,17). These trade-offs can have significant therapeutic implications and are observed in various related fields, including antibiotic resistance (18–21) and cancer treatment (22–25). Thus, elucidating trade-offs associated with bacterial adaptations in the inflamed gut may offer insight into potential collateral effects on bacterial fitness, and prove useful for developing novel treatment strategies based on evolutionary principles.

In this study, we investigated the evolutionary dynamics of resident gut bacteria during intestinal inflammation using an established gnotobiotic mouse model of IBD (26). Through the monocolonization of both *Interleukin 10*-knockout and wildtype mice with a single *E. coli* strain (NC101), this setup allowed us to track genetic and phenotypic changes over the

course of intestinal inflammation and to evaluate their potential clinical relevance. By employing multiomic analysis and high-throughput phenotypic screening, we identify genetic changes in bacteria, alterations in the metabolome, and differences in numerous phenotypic traits among bacterial populations that are specifically associated with evolution in inflamed *Il10*-knockout mice. Remarkably, among the phenotypic changes observed in inflammation-adapted bacteria are sensitivities to antibiotics with known therapeutic value in IBD. These results further confirm the importance of understanding bacterial adaptation to inflammation and suggest its more widespread study in patients as a means to develop novel treatment approaches.

Results

Gnotobiotic model of intestinal inflammation

In order to capture the evolutionary dynamics of bacteria evolving in the context of intestinal inflammation, we implemented a previously established gnotobiotic model, for which inflammation develops upon colonization with the *E. coli* NC101 strain in IL10-deficient (*Il10*$^{-/-}$; herein "KO"), but not wild type (WT) mice (26). We performed two independent *in vivo* experiments (see Methods), in which WT (total N=14) and KO (total N=11) mice were monocolonized and monitored over a period of 12 weeks, with longitudinal sampling of feces for downstream multiomic analyses (Fig 1A; Table S1). Inflammation was monitored via levels of lipocalin-2 in feces, which steadily and significantly increased in KO, but not WT mice, already at one week post-inoculation (Fig 1B, Tables S2 and S3, Wilcoxon signed-rank test Benjamini-Hochberg-corrected $P < 0.05$). Histopathologic assessment of colonic tissue at endpoint reveals significantly higher pathology scores in KO mice than in WT mice (Fig 1C, Kruskal-Wallis H test Benjamini-Hochberg-corrected $P < 0.05$), further confirming that inflammation was specific to KO mice. The bacterial load in the fecal samples was stable throughout the experiment, as measured by CFU counts normalized by feces weight (Fig S1, Tables S4 and S5).

Bacterial populations show genetic diversification in healthy and inflamed mice

To test for genetic diversification of the bacterial populations during the evolution experiment, we performed shotgun sequencing on all bacterial populations at weeks 1, 4, 8, and 12, and identified mutations by comparison with the genome of the ancestral strain. No statistically significant difference was observed in the number of mutations in the bacteria from KO and WT mice at any point in the experiment, suggesting that differences in the intestinal environment in which the populations evolved did not exert a measurable effect on the number of mutations (Fig S2, Table S6). Comparison of the evolved populations at week 12 to the ancestral strain reveals a median number of 43 mutations per mouse in WT and 44 in KO mice (Fig 1D). This indicates that the evolved bacterial populations in both groups of mice genetically differ from the ancestral strain.

To test for overall differences in the mutations that accumulated in bacterial populations that evolved in the WT and KO mice, we performed a partial least-squares discriminant analysis (PLS-DA) on all mutated loci (genes or intergenic regions differing in their nucleotide sequence compared to the ancestor). We find a clear and significant distinction between the populations that evolved in the two mouse genotypes (Fig 1E, PERMANOVA $P = 0.0004$). The

same result was observed when comparing single mutated genomic positions between evolved bacterial populations from WT and KO mice (Fig S3).

Single nucleotide polymorphism differentiates evolved bacteria of all inflamed mice from evolved bacteria of healthy mice

To identify candidates for genetic changes that may be specifically selected in an inflamed environment, we focused on parallel mutations (i.e., genes or intergenic regions that are mutated in at least two mice of the same genotype) and their associated functions. Analysis of the KEGG pathways encompassed by these loci reveals 9 pathways unique to the bacterial populations from inflamed mice (Fig 2A). These pathways include those for lipopolysaccharide biosynthesis, amino acid metabolism, pyruvate metabolism, and oxidative phosphorylation, all of which have been associated with IBD in clinical settings (27–29). Other than the pathways affected only in bacterial populations from the inflamed mice, 17 pathways are affected only in populations from the healthy mice, and 17 other pathways are mutated in populations from both healthy and inflamed mice (Fig 2A).

Univariate analysis reveals that only one particular locus is mutated at significantly higher frequencies in evolved bacterial populations from inflamed than healthy mice (Wilcoxon signed-rank test, corrected $P = 0.001$, Table S7), which is a single nucleotide polymorphism (SNP) (C>T) nine nucleotides upstream of the gene *mprA* (position 3009211) (Fig 2B). It is found in 11/11 KO mice at the endpoint with a frequency between 0.373 and 1, in comparison to 2/14 WT mice with a frequency between 0.085 and 0.239. Two other mutations are detected in the same intergenic region, although in a few populations only. The bacteria from one WT mouse harbors a C>A mutation at the same position (3009211) with a frequency of 0.052, while those from one inflamed mouse harbors a G>T SNP at a nearby position (3009194) with a frequency of 0.611.

To further investigate the most frequent C>T mutation, we analyzed its frequency over the course of the experiment (weeks 1, 4, 8, and 12). At week 1 the mutation is not present or below the detection threshold (minimum frequency of 0.05; see Methods), while at week 4 it is observed in 7/11 KO mice with a maximum frequency of 0.616, in comparison to 1/14 WT mice with a frequency of 0.364 (Fig 2C). After a steady increase in frequency at weeks 8 and 12, the mutation reaches fixation or near fixation in 7/11 KO mice, and is also present at intermediate frequencies in the remaining 4/11 KO mice (Fig 2C). Importantly, the rise in frequency of the C>T mutation strongly coincides with the increase in inflammation as measured by lipocalin-2 levels, both in KO mice alone, and when including all mice (Fig 2C, Fig S4; Spearman's rank correlation rho $P = 0.00005$ for KO mice alone and $P = 3.005e-11$ for all mice).

Interestingly, closer inspection of the intergenic region between the hypothetical protein_02879 and the gene *mprA* reveals this genomic region to be a mutational hotspot, with six positions in this region having mutated over the course of the *in vivo* experiment (Fig S5).

Taken together, we identify a C>T change at position 3009211 in the *E. coli* genome, a parallel mutation significantly associated with intestinal inflammation. The mutation is located upstream of *mprA*, a transcriptional repressor of multiple genes including those

encoding the efflux pump EmrAB. As parallel mutations are a strong indication for adaptation by natural selection, we hypothesized that the evolved bacterial populations have a fitness advantage in the environment they evolved in, and thus next focused on the phenotypes present in the evolved bacterial populations.

Increase in fitness of evolved bacteria in an inflammatory environment

To test whether evolution in the inflamed mouse gut confers a fitness advantage to *E. coli*, we performed "reciprocal transplant" experiments based on *ex vivo* assays using filtered cecal content from inflamed versus non-inflamed mice, collected after sacrifice (referred to subsequently as "*ex vivo* media"). Populations of *E. coli* from fecal samples collected at week 12 from a subset of mice (N = 5 KO mice and N = 5 WT mice) were cultured in *ex vivo* media derived from both inflamed and non-inflamed mice. While no significant difference is observed between bacteria from WT and KO mice when grown in non-inflamed *ex vivo* media (Kruskal-Wallis test $P = 0.9168$; Fig 3A), bacteria from KO mice grow significantly better than those from WT mice in the inflamed *ex vivo* media (Kruskal-Wallis test $P = 0.009023$). Notably, bacteria from KO mice grow significantly better in the inflamed *ex vivo* media than in the non-inflamed *ex vivo* media (Kruskal-Wallis test $P = 0.0472$), while bacteria from the WT mice show no difference in growth in the two media (Kruskal-Wallis test $P = 0.4647$). Thus, bacteria that evolved in the inflamed gut possess a fitness advantage in the inflamed gut environment, suggesting that evolution in the inflamed gut results in specific adaptation to that environment.

Inflamed gut environment displays an altered metabolomic profile

To gain a better understanding of the environment to which these bacteria are adapted, we next performed metabolomic analysis of fecal samples spanning the experimental time course (weeks 1, 2, 5, 6, 10, and 12) using 1H-NMR in mice from one of the two experiments. While WT and KO mice initially display very similar fecal metabolomes (PERMANOVA $P = 0.754$), with time, the fecal metabolic composition begins to vary concurrently with the onset of inflammation and frequency of the C>T SNP upstream of *mprA* (Fig 3B, 1B, 2C). By week 12 of the evolution experiment, the WT and KO mice exhibit notable differences in their fecal metabolomes, as revealed by PLS-DA (PERMANOVA $P = 0.001$; Fig 3B). Among the 77 metabolite features initially found in the samples from week 1, none show significantly different abundances between WT and KO mice. In contrast, in the week 12 samples, 59 of the 77 detected features exhibit significant differences in abundance between the WT and KO mice (Benjamini-Hochberg corrected $P < 0.05$; Tables S8 and S9). Notably, 42 are significantly more abundant in the KO than in WT mice, including all detected amino acids that were significantly enriched in KO mice based on KEGG pathway analysis of parallelly mutated loci. Among the 17 enriched features in WT mice, most are putatively annotated as (poly-)saccharides (Fig S6). Notably, the variations in fecal metabolic composition at week 12 could arise from changes in both the host, linked to inflammation-related changes, and the bacterial population, associated with bacterial adaptation to inflammation.

Phenotypic profiling of evolved bacteria compared to ancestor

Having established that the environment in which the bacteria evolved significantly differs according to mouse genotype, we next focused on specific bacterial traits that may have changed as a consequence of adaptation. Accordingly, we tested the metabolic activity of

the *E. coli* populations using the Biolog GENIII test panel, which comprises 94 unique biochemical tests including a range of compounds (e.g., sugars, amino acids, and short-chain fatty acids), conditions (e.g., different pH and salt concentrations) and chemical sensitivities (e.g., antibiotics; see Methods). Similar to the pattern observed for the fecal metabolome, the overall bacterial metabolic activity across all tested conditions is similar among populations derived from the WT and KO mice at week 1 of the experiment (PERMANOVA $P = 0.519$), as also evidenced by the overlapping of the groups in the PLS-DA based on the overall metabolic activity observed in the BIOLOG GENIII tests (Fig 3C). However, by week 12, the overall pattern of metabolic activity across all tested conditions significantly differs between bacteria from KO and WT mice (PERMANOVA $P = 0.005$). These results suggest that adaptation to the inflamed intestine results in significantly altered bacterial metabolism and ability to grow in presence of different inhibitors. Among the compounds included in this screen, bacteria from WT and KO mice from week 1 showed significantly different metabolic activity in only one compound. In contrast, bacteria from WT and KO mice at week 12 display significantly different metabolic activities in the presence of 31 compounds (Wilcoxon signed-rank test, corrected $P < 0.05$; Tables S10 and S11, Fig S7).

To determine whether the differences in growth observed among the 31 compounds at week 12 may relate to the altered metabolomic environment of inflamed mice, we next compared our BIOLOG GENIII results to the compounds found to be enriched in the fecal metabolome of the KO mice. Interestingly, metabolomics analysis revealed a significant enrichment of the amino acid histidine in the feces of KO mice compared to that of WT mice (Fig S6). In our *in vitro* metabolic assay, we found that bacteria adapted to the inflamed intestine were capable of significantly better metabolic activity in the presence of histidine than bacteria adapted to the healthy intestine (Fig S7). Thus, adaptation to an environment enriched in histidine may have conferred a higher metabolic activity in the presence of this amino acid.

To further explore how the results of our *in vitro* phenotypic analyses may relate to the fecal metabolomic profile observed *in vivo*, we performed a shortest path analysis on the metabolic network of the genome scale metabolic model of *E. coli* NC101 (30) using the metabolomic data and the data from the *in vitro* metabolic activity screen (BIOLOG plates; see methods). Pairs of compounds from the two datasets that are converted easily to each other by means of pathway length include glutamate and L-arginine (Fig 3D, Table S12). Glutamate is significantly more abundant in the feces of the inflamed mice (Fig S6), while bacteria adapted to the inflamed intestine are capable of significantly higher metabolism in the presence of L-arginine (Fig S7). This result suggests that the bacteria may be converting arginine to glutamate, resulting in the enrichment of glutamate in the KO mice (Fig 3D, Table S12). A second pair of compounds showing the same pattern are taurine and L-arginine. However, analysis of the potential pathways between these compounds through a flux variability analysis revealed that taurine cannot be produced by *E. coli* NC101 under any of the tested conditions (Fig S8). Additionally, taurine abundance increased steadily over time only in KO mice (Fig S9). Thus, taurine is most likely produced by the host.

Finally, we examined the 31 significant differences in metabolic activity observed between bacteria from WT and KO mice at week 12 in light of their potential clinical value. A first compound of interest is N-acetyl beta-D mannosamine (NADM), which is a precursor to

sialic acid and was shown to promote the *E. coli* colonization of the inflamed gut (31). Our *E. coli* populations show higher levels of metabolic activity in the presence of NADM after adaptation to the inflamed mouse gut. In contrast, *E. coli* evolved in the non-inflamed mouse gut show no such change (Fig 4). These findings suggest that increased virulence may arise in the context of adaptation to an inflamed environment.

A second interesting candidate is lithium chloride, which is known to have anti-inflammatory effects via the inhibition of a key host regulator of inflammation, glycogen synthase kinase-3 beta (32). In our experiment, bacterial populations evolved in WT mice display improved metabolic capacity in the presence of lithium chloride compared to the ancestor, while no such change is observed among those evolved in the KO mice. Thus, our results suggest that the inflamed intestinal environment may prevent the acquisition of this phenotype in *E. coli*.

A final promising category of candidates are antibiotics, including fusidic acid, vancomycin, and lincomycin. All three of these antibiotics contributed to the overall significant difference in metabolic activity of the bacteria from WT and KO mice (Fig 3C, Fig S10), and fusidic acid is also significant between bacteria from the two mouse genotypes in univariate analysis (Wilcoxon signed-rank test, corrected $P < 0.05$). Fusidic acid is an antibiotic that targets gram-positive bacteria and is commonly used to treat skin infections (33). Interestingly, it was also shown to be effective in reducing disease activity in a small number of Crohn's disease patients, thought to be due to its immunosuppressive properties (34,35). We observe *E. coli* to display decreased metabolic activity in the presence of fusidic acid after adaptation to the inflamed intestine, but increased metabolic activity after adaptation to the healthy intestine. These results suggest a potential trade-off between adaptation to inflammation and resistance to fusidic acid, where *E. coli* adapted to inflammation also show lower resistance to fusidic acid.

In summary, we observe widespread phenotypic differences among bacterial populations that evolved in the inflamed intestines of KO mice, compared to non-inflamed WT mice. These results relate to differences in the metabolome between these two intestinal environments, and include phenotypes that carry the potential for exploitation in a clinical setting.

Discussion

In this study, we describe the findings of an *in-vivo* bacterial evolution experiment in a gnotobiotic mouse model of IBD. We find that *E. coli* evolved in the inflamed mouse gut accumulated specific genetic changes, and that these changes confer a fitness advantage in the inflamed intestinal environment, which significantly differs in its metabolome. Finally, we showed that adaptation to the inflamed intestine also resulted in several phenotypic differences that may carry clinical relevance, such as differential tolerance to antibiotics.

Recent studies have brought to light how strain-level changes in members of the gut microbiome can play a crucial role in the adaptation of the gut microbiome to novel conditions in the gut (14,36,37). However, the effect of inflammation on the evolution of gut commensals remains largely unexplored. Barreto et al. (2020) followed the adaptation of *E.*

coli in mice of different ages *in vivo* (14). They showed that the aged mouse gut, which also showed high levels of inflammation, was a more stressful environment for *E. coli*, resulting in a higher number of mutations and more severe selective pressure on the commensals, particularly in bacterial loci associated with stress-related functions. Notably, we find no difference in the number of mutations acquired by *E. coli* in our inflamed mice, suggesting that other factors associated with aging may contribute to the increased bacterial mutation rate observed by Barreto et al. (2020) (14).

More recently, Tawk et al. (2023) conducted a study of mice monocolonized with *Bacteroides thetaiotaomicron* that were subsequently infected by *Citrobacter rodentium* and developed inflammation. In this setting, a single-nucleotide variant of *B. thetaiotaomicron*, which had a higher tolerance to oxidative stress than the ancestral variant, underwent selective sweeps and came to dominate the intestinal community (37). Although the experimental setup and duration of inflammation differs between this and the current study, our candidate mutation is also known to be associated with oxidative stress (38). This is thus consistent with the observations by both Barreto et al. (2020) and Tawk et al. (2023) (14,37), and suggests oxidative stress to be a key selective pressure in an inflamed environment. Moreover, oxidative stress is known to be a major player in the pathophysiology of IBD (39).

Importantly, many of our findings are consistent with observations made in clinical IBD settings. First, the KEGG pathways affected by parallel mutations specific to the inflamed mice (Fig 2A) include lipopolysaccharide biosynthesis (involved in the activation of the immune system in IBD) and D-amino acid-, pyruvate-, and thiamine metabolism. This is in line with previous reports of basic metabolism being reduced in IBD (28,40). Similarly, oxidative phosphorylation pathways were reported to be reduced in patients with UC (27,29).

Second, the metabolomic profiling of the fecal samples reveals that KO mice have significantly higher levels of many amino acids, which was also reported in IBD patients (41). Furthermore, the results of our shortest path analysis suggest that bacterial production of glutamate from arginine may underlie the enrichment of glutamate in the inflamed gut. Although taurine-arginine was also one of the shortest paths we found, taurine could not be produced by *E. coli* according to the flux variability analysis. Thus, taurine is most likely produced by the host. Taurine is known to be a promoter of colonization resistance, and infection was shown to prime the microbiota against subsequent infections by inducing host production of taurine (42). Indeed, taurine was also reported to ameliorate inflammation in rat models of inflammation (43). Furthermore, taurine is a substrate for microbiota-driven production of hydrogen sulfide (44), and arginine is a precursor to polyamines that can protect against reactive species such as hydrogen sulfide (45). Thus, the bacterial adaptation for improved metabolic activity in the presence of arginine may be a response to host-induced inflammatory changes in the intestine.

Third, *E. coli* adapted to the inflamed mouse gut also showed some clinically relevant phenotypes (Fig 4). N-acetyl beta-D mannosamine (NADM) is a precursor of polysialic acid, a pathogenic determinant, and studies showed that it can promote the colonization of the inflamed intestine by pathogenic *E. coli* (31,46). As NADM is a crucial player in mediating

pathogenic activity in the inflamed intestine, the improved metabolic activity of inflammation-adapted *E. coli* we observe in the presence of NADM may be a phenotype associated with virulence. This is consistent with reports of virulence-associated phenotypes such as hypermotility being selected for during the evolution of an adherent-invasive *E. coli* in the inflamed mouse gut (13). Further, lithium chloride is known to inhibit the activity of glycogen synthase kinase 3-β, a master regulator of host chronic intestinal inflammation mediated through toll-like receptors, and was used as a treatment in a mouse model of IBD (32,47). The effect of lithium on the microbiome is not yet elucidated. *E. coli* tolerance to lithium ions is regulated through antiporters, and proline has been shown to induce the uptake of lithium ions by *E. coli* (48,49). Our finding that adaptation to the healthy mouse intestine confers improved metabolic capacity in the presence of lithium chloride, while adaptation to the inflamed intestine does not (Fig 4), implies that lithium may affect both the host and microbiome. It may also imply that adaptation to the healthy intestine affects the antiporter-dependent detoxification system of *E. coli*, resulting in improved ion tolerance.

Lastly, we found that bacterial adaptation to the inflamed gut decreases metabolic activity in the presence of fusidic acid, while adaptation to the healthy mouse gut improved metabolic activity in the presence of fusidic acid (Fig 4). Fusidic acid is an antibiotic with T-cell-specific immunosuppressive effects that also stimulates gastric mucus secretion. Furthermore, it was successfully applied for alleviating inflammation in rats, as well as for treating selected Chron's disease patients for whom conventional treatment was ineffective (34,35). However, the effect of fusidic acid on the gut microbiome in IBD has not been studied. Our results imply that bacterial adaptation to the inflamed gut can result in a trade-off for resistance to fusidic acid. Importantly, such trade-offs are a fundamental concept in evolutionary medicine, where increased fitness in one context results in a consequent decrease in fitness in another context, and are proposed as possible potent therapeutic strategies against antibiotic resistance and cancer (18,50). Thus, the therapeutic effect of fusidic acid observed in Chron's disease patients is due to trade-offs surrounding microbiome adaptation to the inflamed gut, and/or its immunosuppressive effects on the host.

Current treatment options for IBD are largely limited to treating the inflammation, with a chronic risk of relapse. Corticosteroids, aminosalicylates, and immunosuppressive agents are the conventional drugs of choice, and the safety and efficacy of novel emerging strategies remain unclear (reviewed in (51)). Given that disease-specific aspects of the microbiome have been shown to remain stable over long periods in IBD patients despite treatment (52), a persistent microbial influence on the intestinal environment may be a key risk factor of relapse. Our results thus highlight new avenues of research involving evolution-informed therapeutic strategies that exploit trade-offs to either prevent adaptation to inflammation and/or help restore desirable ancestral traits in the microbiome.

Methods

Bacterial strains

E. coli NC101 strain was obtained from Balfour Sartor, University of North Carolina, Chapel Hill, NC, USA (53). The strain was cultured at 37 °C in Luria Bertani (LB) medium in continuous shaking. The ancestor strain for the setup of the *in vivo* experiment was obtained by plating the overnight culture on LB agar, and by picking single colonies to be used as inocula for the *in vivo* evolution experiment.

Mouse model

To study *E. coli* adaptation to the inflamed gut, two independent experiments were set up. Germ-free (GF) C57BL/6NTac (WT) and C57BL/6NTac-Il10em8Tac (KO) male mice were purchased from Taconic Biosciences (Silkeborg, Denmark) and housed in the Germ-Free Animal Facility at the Max Planck Institute for Evolutionary Biology (Ploen, Germany). GF mice were maintained in sterile isolators (MB-10, Quip Laboraties, Delaware, USA), fed on sterilized 50 kGy V1124-927 Sniff (Soest, Deutschland). The animals were allocated in independent cages with a maximum of 4 mice per isolator until they reached an age of 12 weeks. Detailed information about the mice used in the study are reported in Table S1. Initially, 19 WT mice and 15 KO mice were monocolonized with the *E. coli* NC101 strain. Only mice that survived for the duration of the experiment (12 weeks; N = 14 WT mice and N = 11 KO mice) were included in the study. The study was performed according to approved animal protocols and institutional guidelines of the Max Planck Institute. Mice were maintained and handled in accordance with FELASA guidelines and German animal welfare law (Tierschutzgesetz § 11, permit from Veterinäramt Kreis Plön: 1401-144/PLÖ-004697).

The strains used as inocula were diluted in sterile PBS and 200 µL (equivalent to 1x10^8 bacteria) were gavaged using a sterile gavage needle (Reusable Feeding Needles 18G, Fine Science Tools, Heidelberg, Deutschland). Fecal pellets were collected in a sterile manner twice a week to study the evolution of *E. coli* for a total of 24 samples collected per mouse and once a week for metabolomic investigations. An overview of the sampling plan is reported in Fig 1A.

Histopathological evaluation

Mice were sacrificed at week 12 and colon tissue was collected and arranged to form a Swiss-roll (54). Hematoxylin and eosin-stained sections of colonic tissue Swiss-rolls were scored by two independent researchers in a blinded manner using the scoring system described by Adolph, et al. (2013) (55). The score is composed of five sub-scores, namely mononuclear cell infiltrate, crypt hyperplasia, epithelial injury or erosion, polymorphonuclear cell infiltrates, and transmural inflammation. Each of the first four sub-scores is awarded a score from 0 to 3, whereas transmural inflammation is scored from 0 to 4, with a higher score indicating a more severe level of inflammatory activity. The sum of the sub-scores is then multiplied by a factor based on the percentage of the bowel length affected (1= < 10%; 2= 10-25%; 3= 25-50%; 4= >50%).

Feces processing

Feces weight and consistency were recorded. Feces were homogenized in 1.5 ml sterile PBS on a horizontal vortexer (Vortex Mixer Modell Vortex-Genie® 2, Scientific Industries, Bohemia, NY, USA) at maximum speed for 30 min, then separated in three aliquots of

500 μL. Each aliquot was centrifuged at 10,000 rpm for 5 min. The supernatants were transferred in a new tube and stored at -20 °C for later lipocalin-2 concentration measurement. One pellet aliquot was resuspended in 500 μL PBS and used to prepare a 12-point 1/10 dilution series that was plated on LB agar. After overnight growth at 37 °C, the CFU were counted to measure bacterial load. The second pellet aliquot was resuspended in 1 ml RNAlater and stored at +4 °C for 24 h, after which the tube was centrifuged at 10,000 rpm for 5 min to remove the RNAlater, and the pellet was stored at -20 °C for subsequent nucleic acid extraction and sequencing. The last pellet aliquot was resuspended in 500 μL of LB containing 20% glycerol and stored at -70 °C for further phenotypic investigation.

Lipocalin-2 quantification

Lipocalin-2 concentration was measured in the supernatants using the commercial kit Mouse Lipocalin-2/NGAL DuoSet ELISA (R&D Systems, Minneapolis, MN, USA) for mouse Lipocalin-2 (DY1857). Testing was performed by following manufacturer's instructions. Samples were diluted 1:10 and added to the plate. The optical density of each well was determined with a plate reader (SPARK, Tecan, Tecan, Männedorf, Switzerland) at 450 nm and 540 nm. Lipocalin-2 concentrations were normalized by the weight of feces for each sample.

Shotgun sequencing

Total DNA and RNA were extracted using ZymoBIOMICS DNA/RNA Mini Kit (Zymo Research, Freiburg, Germany), following producer's instructions from fecal pellets collected at weeks 1, 4, 8, and 12, as well as from the *E. coli* NC101 cultures that served as inocula. Shotgun metagenomics sequencing was performed on four Illumina Nextseq (HighOutput 300 cycles) sequencing run at the Max Planck Institute for Evolutionary Biology (Plön, Germany).

Raw reads were filtered and trimmed to ensure good quality with Cutadapt (version 3.2; (56)). First, any pair containing Ns or homopolymers (10 nucleotides or more), or that were longer than 151 bp were discarded. Then sequences were trimmed with a quality cut-off of 25 at both ends for both reads, Illumina adapters were removed and sequences shorter than 50 bp were discarded. Good quality sequences were then filtered to exclude mouse sequences (mouse_C57BL) using KneadData (58). A final filter was applied to remove any adapter leftovers with Trimmomatic (57) and sequences shorter than 105 bp were discarded. Mutations were identified using Breseq (59) by comparing the obtained metagenomes with the reference genome of *E.coli* NC101, using default options. Gdtools was used to compare mutations in the samples.

Measurement of the metabolic activity of bacteria

To investigate the metabolism of the evolved populations, we used Biolog GENIII MicroPlates (Biolog, Hayward, CA). Evolved populations stored in glycerol were inoculated onto the Inoculation Fluid-A (IF-A) provided by the manufacturer such that the OD_{600} was between 0.02-0.05. After adjusting the OD_{600}, the inoculated IF-A was shaken well and distributed into the Biolog GENIII MicroPlate (100 µl into each well). The plate was then covered by a sterile Breathe-Easy membrane (Sigma-Aldrich, St. Louis, MO) and placed into a plate reader (SPARK, Tecan, Männedorf, Switzerland) with a preset temperature of 37 °C.

The plate reader was then run with the following parameters: temperature: 37 °C, shaking: 250 rpm, OD_{590} measurement: every 15 min, total running time: 36 h. From the OD_{590} measures, area under the curve (AUC) was used as a proxy for metabolic activity. The Biolog assay was repeated for populations from fecal samples collected at weeks 1 and 12 from all 25 mice, with two replicates each.

Ex vivo *assay*

Cecal content was collected from each mouse during the dissection at the end of the second experiment. The amount of cecal content from each mouse was different, based on the amount that was in the cecum at the time of the dissection. Sterile PBS was added to the cecal content, the volume being adjusted based on the amount of cecal content collected for each mouse (20 mg/ml). The protocol was adapted from Kitamoto et al. (2020) (60). The PBS-cecal content mixture was centrifuged twice (once at 500*g* for 5 min and again at 10000*g* for 5 min) and then filter-sterilized through a 0.2 µm filter. The *ex vivo* medium from each mouse was mixed well, and 100 µL was spread onto an LB agar plate to ensure they were sterile. The *ex vivo* media from all healthy mice were pooled, as was the *ex vivo* media from all inflamed mice, resulting in two *ex vivo* media. Populations from fecal samples collected at week 12 from a subset of mice (n = 5 KO and n = 5 WT mice) were inoculated into the *ex vivo* media and incubated in the TECAN Spark plate reader with a preset temperature of 37 °C. The plate reader was then run with the following parameters: temperature: 37 °C, shaking: 250 rpm, OD_{600} measurement: every 15 min, total running time: 36 h. From the OD_{600} measures, area under the curve (AUC) was used as a proxy for growth.

Metabolomic evaluation of the fecal pellets

During the second experiment, samples for metabolomic investigation were collected once per week and snap frozen in liquid nitrogen. Samples were stored at -70 °C and delivered at Helmholtz Center Munich for metabolomic investigation. The non-targeted metabolomics approach of mouse fecal samples was undertaken using NMR spectroscopy. To extract the aqueous metabolites, we homogenized 2-3 fecal pellets in 1 mL H_2O using ceramic beads (NucleoSpin, Macherey–Nagel, Dueren, Germany) and a TissueLyser (Qiagen, Hilden, Germany) mixing the sample for 3 x 30 s at 4,500 rpm with a 10 s cooling break (< 0°C). Subsequently, the homogenate was centrifuged (13,000 rpm for 10 min at 4 °C), the supernatant evaporated with a SpeedVac, and the dried extract reconstituted in 200 µL NMR buffer (10% D_2O, 100 mM phosphate buffer with 0.1% trimethylsilyl-tetradeuteropropionic acid (TSP), pH 7.4). Samples were transferred to 3 mm NMR tubes and immediate NMR analysis was performed in a randomized order with a Bruker 800 MHz spectrometer operating at 800.35 MHz equipped with a Bruker SampleJet for sample cooling (283 K) and a QCI-cryogenic probe. A standard one-dimensional pulse sequence (noesygppr1d) delivered an overview of all molecules. The acquisition parameters were as follows: water suppression irradiation during recycle delay (2 s), mixing time = 200 ms, 90◦ pulse = 12.5 µs. We collected 512 scans into 64 K data points with a spectral width of 12 ppm. The software TopSpin 3.6 (Bruker BioSpin, Ettlingen, Germany) was used for processing, i.e., Fourier transformation, manual phasing, baseline correction and calibration to TSP (δ 0.00). Data were imported into Matlab software R2011b (Mathworks, Natick, MA, USA) and further processed, i.e., the water region removed, baseline adjusted (61) and

spectra normalized (62). Relative quantification of metabolites was done using the peak height of selected peaks and compounds identified as described in our published workflow (63).

Shortest path analysis

For the shortest path analysis, we used the metabolic model reconstructed in the AGORA2 resource for the human microbiome (30). The model was translated into a graph with metabolites as nodes, and the reactions converting metabolites into one another as edges. The shortest path analysis was performed using the Dijkstra algorithm implemented in the igraph package (1.3.5) of R (4.2.2) (64,65). To avoid shortcuts through the network by using cofactors as intermediate compounds, the edges were weighted by the sum of degree of the nodes it connected, as suggested by Faust et al. (66). For each compound from the *in vitro* screen, we calculated a set of shortest paths to all other metabolites in the model. Each value in the set was the average shortest path of the five shortest paths between two metabolites – this was done to account for uncertainties in pathway calculation based on only the network properties. For our analysis, we only considered pathways between compounds from the two datasets, which were among the shortest 5% pathways in a pathway set.

Statistical investigation

Statistical analyses were performed using packages in RStudio 2023.03.0+386. For PERMANOVA analyses, adonis was used (67) on Bray-curtis distances of the data (68), and mixomics was used for PLS-DA (69). AUCs were calculated using desctools (70).

Figures and figure legends

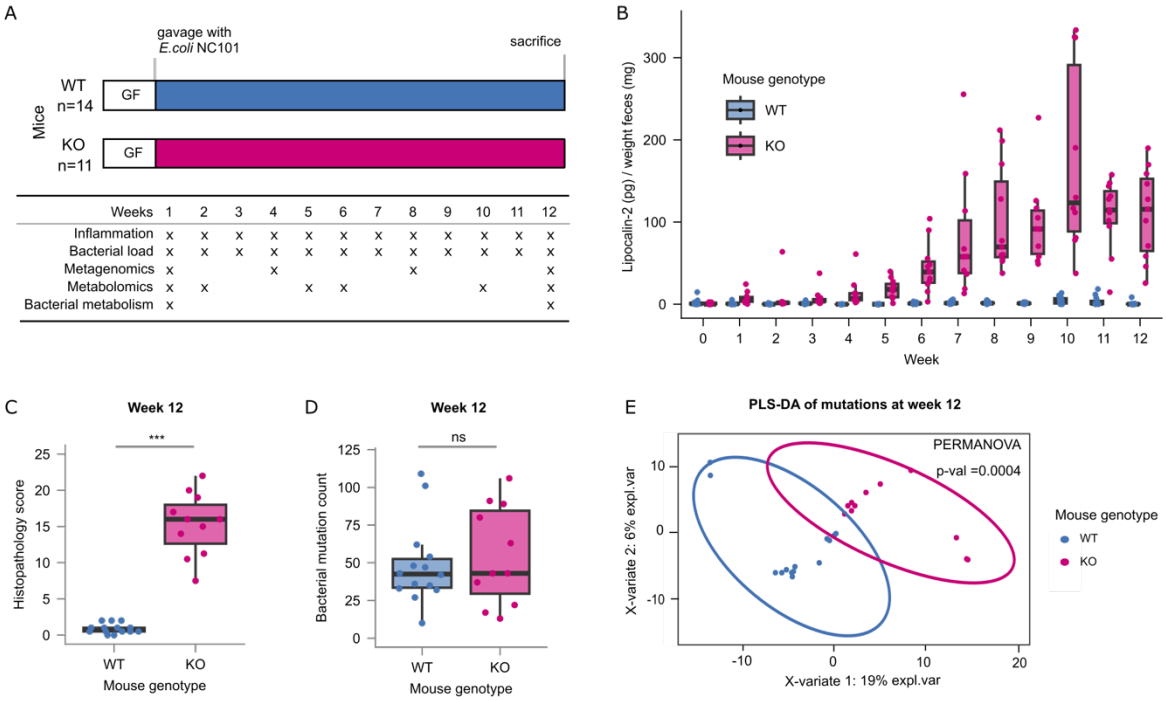

Figure 1. Application of a mouse model of IBD to test the effect of gut inflammation on the evolution of NC 101

A Schematic of the experimental setup. Germ-free WT and *Il10*$^{-/-}$ mice were monocolonized with *E. coli* NC101. Fecal samples were collected from each mouse at the indicated time points and analyzed as described. **B** Fecal lipocalin-2 levels from the WT and *Il10*-/- mice. Lipocalin-2 was measured based on Mouse Lipocalin-2/NGAL DuoSet ELISA and normalized by feces weight. Each dot represents one mouse at each sampling point. Results of Wilcoxon signed-rank test of lipocalin-2 concentrations at each time point are reported in Table S3. Differences were considered statistically significant at Benjamini-Hochberg-corrected P <0.05. **C** Boxplots of histopathology scores of the colon tissue of the mice after sacrifice at the end of the experiment. Each dot represents one mouse. Differences were considered statistically significant with Kruskal-Wallis H test at Benjamini-Hochberg-corrected P <0.05. **D** Number of mutations in the bacterial populations at week 12 week in WT and KO mice compared to the reference genome. Each dot represents the bacterial population from one mouse. Differences were considered statistically significant with Kruskal-Wallis H test at Benjamini-Hochberg-corrected P <0.05. **E** Partial least squares-discriminant analysis of the mutated genomic locations in the evolved populations of *E. coli* NC101 at week 12 in WT and KO mice gut compared to the reference genome. Differences were considered statistically significant at PERMANOVA P < 0.05.

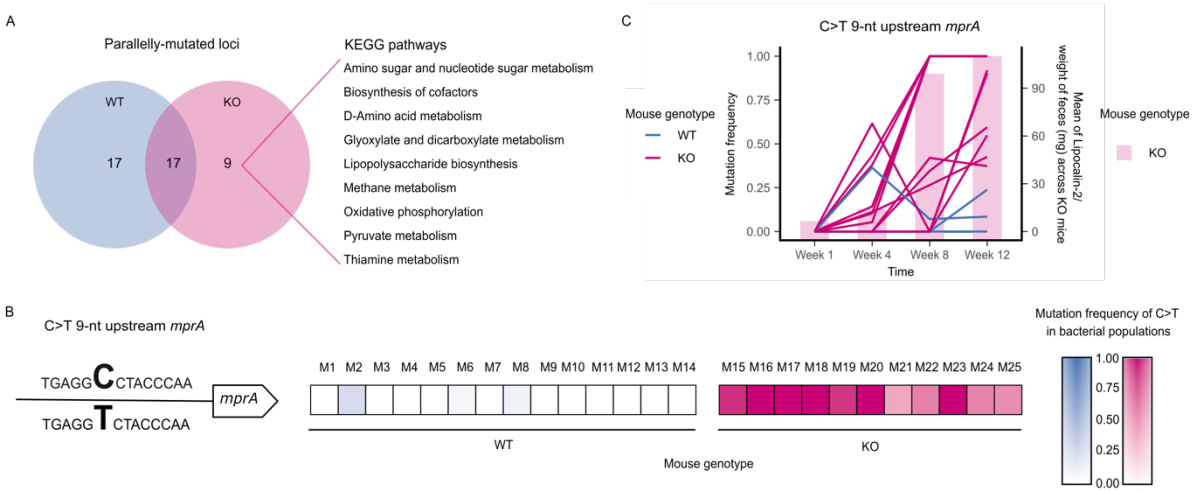

Figure 2. Parallel evolution of *E. coli* in inflamed mice revealed a disease-specific genetic signature A Parallelly mutated loci were classified based on KEGG pathways; **B** An intergenic C>T mutation 10-nt upstream of *mprA* was the unique parallel mutation significantly more abundant in populations evolved in the inflamed gut (Wilcoxon signed-rank test Benjamini-Hocheberg corrected $P < 0.005$). The heatmap shows the frequency of the mutation in bacterial populations from each mouse. **C** Mutation frequency (left axis) of the intergenic C>T mutation 10-nt upstream of *mprA* and mean of lipocalin-2 concentrations across KO mice at different timepoints during the *in-vivo* evolution experiment. Each line represents a population from a single mouse. Each bar represents the mean value of the normalized concentration of lipocalin-2 in fecal samples from KO mice.

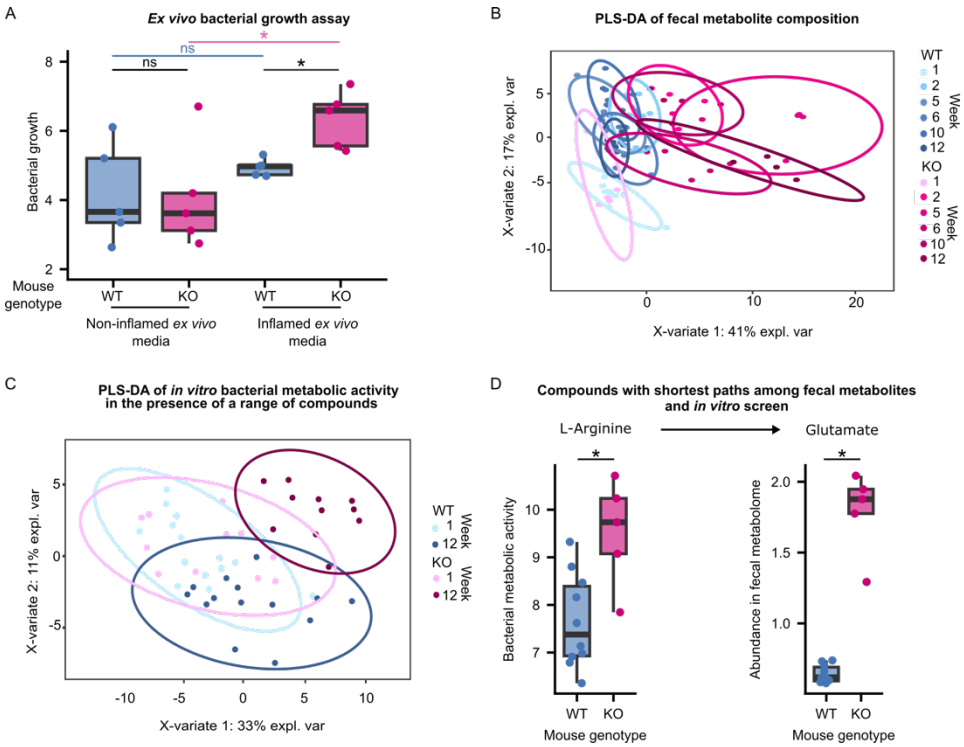

Figure 3. Phenotypic characterization of evolved *E. coli* and the inflammatory environment in which they were selected.

A Evolved populations from a subset of mice (n = 5 KO mice and n = 5 WT mice) were cultured in media derived from the cecal content collected from the healthy (WT) and inflamed (KO) mice after sacrifice. Area under the curve (AUC) calculated from growth curves measured during the growth of evolved populations from each mouse in inflamed and healthy cecal content is shown. Each dot is the mean of three independent replicates. *, $P < 0.05$ (Kruskal-Wallis H test), ns, not significant **B** Partial least squares discriminant analysis (PLS-DA) of the fecal metabolite abundances at different time points during the evolution experiment. Differences were considered statistically significant at PERMANOVA $P < 0.05$ **C** Bacterial metabolism was measured *in- vitro* in a range of compounds. Measurements were performed on bacterial populations derived from fecal samples collected at weeks 1 and 12 of the *in-vivo* evolution experiment. Partial least squares discriminant analysis (PLS-DA) was performed on the area under the curves (AUCs) of the measured metabolic activity of the evolved bacterial populations from all mice in the range of compounds. Differences were considered statistically significant at PERMANOVA $P < 0.05$ **D** Compounds from the fecal metabolome and the *in vitro* screen that had the shortest path were inspected. One of the pairs with shortest paths was glutamate-arginine. Glutamate was enriched in the fecal metabolome of KO mice, while KO-adapted bacteria showed higher metabolic activity in the presence of arginine. Each dot represents the abundance of the compound in the fecal sample from a mouse (for glutamate) or the mean metabolic activity of the bacterial population from a mouse in the presence of L-arginine from two independent measurements (for arginine). *, $P < 0.05$ (Kruskal-Wallis test at Benjamini-Hochberg-corrected), ns, not significant.

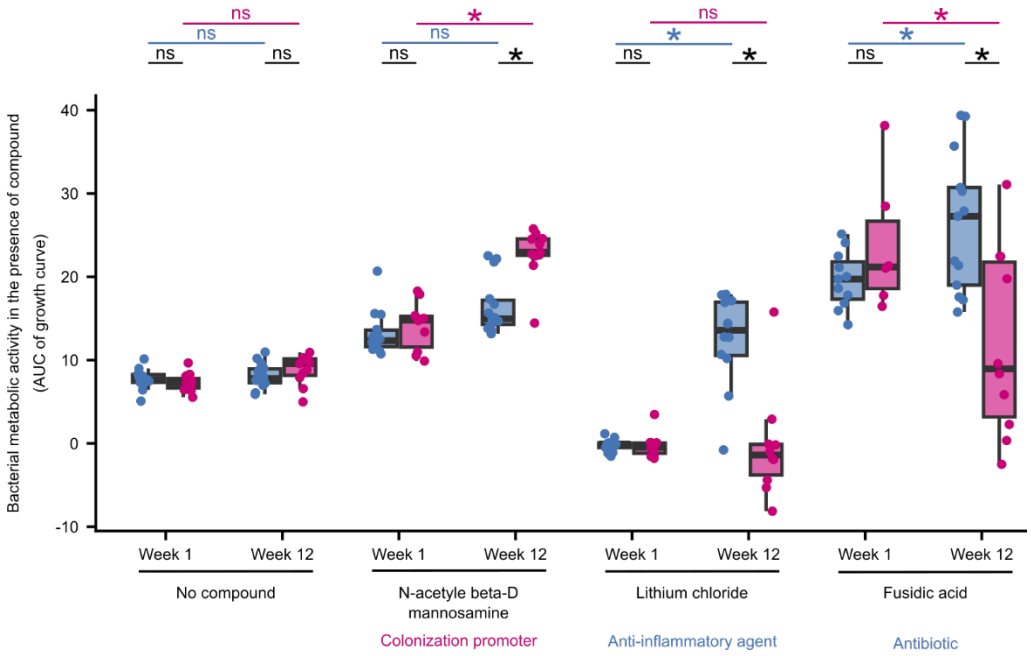

Figure 4. *E. coli* adapted to the inflamed gut show phenotypes with clinical relevance. Metabolic activity of bacteria isolated at weeks 1 and 12 of the evolution experiment in the presence of three selected compounds. Area under the curve was calculated from growth curves measured during the growth of evolved populations in the presence of each compound. Each dot represents the mean of two independent replicates of the metabolic activities of the *E. coli* population from a mouse measured in two independent experiments. *, $P < 0.05$ (Kruskal-Wallis test at Benjamini-Hochberg-corrected). The clinical relevance of the three compounds is indicated.

Acknowledgments

We are grateful to Balfour Sartor for providing the NC101 *E. coli* strain, the MPI-Plön mouse team for support with animal experiments, Sven Künzel for excellent technical support, Britt Marie Hermes for support in manuscript preparation, and Wael Elhenawy and Isabel Gordo for helpful and constructive discussions.

Funding

The study was supported by the Deutsche Forschungsgemeinschaft (DFG) Research Unit FOR5042 “miTarget – The Microbiome as a Target in Inflammatory Bowel Disease” (subprojects P10, Z, and INF) and Cluster of Excellence 2167 “Precision Medicine in Chronic Inflammation” (grant no. EXC2167). RU was additionally funded by the International Max-Planck Research School for Evolutionary Biology (IMPRS EvolBio). Work in the Unterweger group is funded by the German Federal Ministry for Education and Research (grant 01KI2020).

References

1. Ott SJ, Musfeldt M, Wenderoth DF, Hampe J, Brant O, Fölsch UR, et al. Reduction in diversity of the colonic mucosa associated bacterial microflora in patients with active inflammatory bowel disease. Gut. 2004 May;53(5):685–93.

2. Gevers D, Kugathasan S, Denson LA, Vázquez-Baeza Y, Van Treuren W, Ren B, et al. The treatment-naïve microbiome in new-onset Crohn's disease. Cell Host Microbe. 2014 Mar 12;15(3):382–92.

3. Rehman A, Rausch P, Wang J, Skieceviciene J, Kiudelis G, Bhagalia K, et al. Geographical patterns of the standing and active human gut microbiome in health and IBD. Gut. 2016 Feb;65(2):238–48.

4. Halfvarson J, Brislawn CJ, Lamendella R, Vázquez-Baeza Y, Walters WA, Bramer LM, et al. Dynamics of the human gut microbiome in inflammatory bowel disease. Nat Microbiol. 2017 Feb 13;2:17004.

5. Schirmer M, Franzosa EA, Lloyd-Price J, McIver LJ, Schwager R, Poon TW, et al. Dynamics of metatranscription in the inflammatory bowel disease gut microbiome. Nat Microbiol. 2018 Mar;3(3):337–46.

6. Schirmer M, Garner A, Vlamakis H, Xavier RJ. Microbial genes and pathways in inflammatory bowel disease. Nat Rev Microbiol. 2019 Aug;17(8):497–511.

7. Willing BP, Dicksved J, Halfvarson J, Andersson AF, Lucio M, Zheng Z, et al. A pyrosequencing study in twins shows that gastrointestinal microbial profiles vary with inflammatory bowel disease phenotypes. Gastroenterology. 2010 Dec;139(6):1844-1854.e1.

8. Barreto HC, Gordo I. Intrahost evolution of the gut microbiota. Nat Rev Microbiol. 2023 Apr 17;

9. Giraud A, Matic I, Tenaillon O, Clara A, Radman M, Fons M, et al. Costs and benefits of high mutation rates: adaptive evolution of bacteria in the mouse gut. Science. 2001 Mar 30;291(5513):2606–8.

10. Paepe MD, Gaboriau-Routhiau V, Rainteau D, Rakotobe S, Taddei F, Cerf-Bensussan N. Trade-Off between Bile Resistance and Nutritional Competence Drives Escherichia coli Diversification in the Mouse Gut. PLOS Genet. 2011 Jun 16;7(6):e1002107.

11. Barroso-Batista J, Sousa A, Lourenço M, Bergman ML, Sobral D, Demengeot J, et al. The First Steps of Adaptation of Escherichia coli to the Gut Are Dominated by Soft Sweeps. PLOS Genet. 2014 Mar 6;10(3):e1004182.

12. Zhao S, Lieberman TD, Poyet M, Kauffman KM, Gibbons SM, Groussin M, et al. Adaptive Evolution within Gut Microbiomes of Healthy People. Cell Host Microbe. 2019 May 8;25(5):656-667.e8.

13. Elhenawy W, Tsai CN, Coombes BK. Host-Specific Adaptive Diversification of Crohn's Disease-Associated Adherent-Invasive Escherichia coli. Cell Host Microbe. 2019 Feb;25(2):301-312.e5.

14. Barreto HC, Sousa A, Gordo I. The Landscape of Adaptive Evolution of a Gut Commensal Bacteria in Aging Mice. Curr Biol. 2020 Mar;30(6):1102-1109.e5.

15. Daniel H. Diet and Gut Microbiome and the "Chicken or Egg" Problem. Front Nutr [Internet]. 2022 [cited 2023 Jul 25];8. Available from: https://www.frontiersin.org/articles/10.3389/fnut.2021.828630

16. Garland T, Downs CJ, Ives AR. Trade-Offs (and Constraints) in Organismal Biology. Physiol Biochem Zool PBZ. 2022;95(1):82–112.

17. Nesse RM, Ganten D, Gregory TR, Omenn GS. Evolutionary molecular medicine. J Mol Med Berl Ger. 2012 May;90(5):509–22.

18. Merker M, Tueffers L, Vallier M, Groth EE, Sonnenkalb L, Unterweger D, et al. Evolutionary Approaches to Combat Antibiotic Resistance: Opportunities and Challenges for Precision Medicine. Front Immunol [Internet]. 2020 [cited 2023 Jul 6];11. Available from: https://www.frontiersin.org/articles/10.3389/fimmu.2020.01938

19. Roemhild R, Schulenburg H. Evolutionary ecology meets the antibiotic crisis: Can we control pathogen adaptation through sequential therapy? Evol Med Public Health. 2019;2019(1):37–45.

20. Andersson DI, Balaban NQ, Baquero F, Courvalin P, Glaser P, Gophna U, et al. Antibiotic resistance: turning evolutionary principles into clinical reality. FEMS Microbiol Rev. 2020 Mar 1;44(2):171–88.

21. Melnikov SV, Stevens DL, Fu X, Kwok HS, Zhang JT, Shen Y, et al. Exploiting evolutionary trade-offs for posttreatment management of drug-resistant populations. Proc Natl Acad Sci U S A. 2020 Jul 28;117(30):17924–31.

22. Hausser J, Szekely P, Bar N, Zimmer A, Sheftel H, Caldas C, et al. Tumor diversity and the trade-off between universal cancer tasks. Nat Commun. 2019 Nov 28;10(1):5423.

23. Zhang J, Cunningham JJ, Brown JS, Gatenby RA. Integrating evolutionary dynamics into treatment of metastatic castrate-resistant prostate cancer. Nat Commun. 2017 Nov 28;8(1):1816.

24. Jacqueline C, Biro PA, Beckmann C, Moller AP, Renaud F, Sorci G, et al. Cancer: A disease at the crossroads of trade-offs. Evol Appl. 2016 Dec 26;10(3):215–25.

25. Cunningham JJ, Gatenby RA, Brown JS. Evolutionary dynamics in cancer therapy. Mol Pharm. 2011 Dec 5;8(6):2094–100.

26. Kim SC, Tonkonogy SL, Karrasch T, Jobin C, Sartor RB. Dual-association of gnotobiotic IL-10-/- mice with 2 nonpathogenic commensal bacteria induces aggressive pancolitis. Inflamm Bowel Dis. 2007 Dec;13(12):1457–66.

27. Schneider AM, Özsoy M, Zimmermann FA, Brunner SM, Feichtinger RG, Mayr JA, et al. Expression of Oxidative Phosphorylation Complexes and Mitochondrial Mass in Pediatric and Adult Inflammatory Bowel Disease. Oxid Med Cell Longev. 2022;2022:9151169.

28. Morgan XC, Tickle TL, Sokol H, Gevers D, Devaney KL, Ward DV, et al. Dysfunction of the intestinal microbiome in inflammatory bowel disease and treatment. Genome Biol. 2012 Sep 26;13(9):R79.

29. Davenport M, Poles J, Leung JM, Wolff MJ, Abidi WM, Ullman T, et al. Metabolic alterations to the mucosal microbiota in inflammatory bowel disease. Inflamm Bowel Dis. 2014 Apr;20(4):723–31.

30. Heinken A, Hertel J, Acharya G, Ravcheev DA, Nyga M, Okpala OE, et al. Genome-scale metabolic reconstruction of 7,302 human microorganisms for personalized medicine. Nat Biotechnol. 2023 Jan 19;1–12.

31. Huang YL, Chassard C, Hausmann M, von Itzstein M, Hennet T. Sialic acid catabolism drives intestinal inflammation and microbial dysbiosis in mice. Nat Commun. 2015 Aug 25;6(1):8141.

32. Hofmann C, Dunger N, Schölmerich J, Falk W, Obermeier F. Glycogen synthase kinase 3-β: A master regulator of toll-like receptor-mediated chronic intestinal inflammation. Inflamm Bowel Dis. 2010 Nov 1;16(11):1850–8.

33. Fernandes P. Fusidic Acid: A Bacterial Elongation Factor Inhibitor for the Oral Treatment of Acute and Chronic Staphylococcal Infections. Cold Spring Harb Perspect Med. 2016 Jan 4;6(1):a025437.

34. Langholz E, Brynskov J, Bendtzen K, Vilien M, Binder V. Treatment of Crohn's disease with fusidic acid: an antibiotic with immunosuppressive properties similar to cyclosporin. Aliment Pharmacol Ther. 2007 Mar 31;6(4):495–502.

35. Kilic FS, Erol K, Batu O, Yildirim E, Usluer G. The effects of fusidic acid on the inflammatory response in rats. Pharmacol Res. 2002 Apr;45(4):265–7.

36. Dapa T, Ramiro RS, Pedro MF, Gordo I, Xavier KB. Diet leaves a genetic signature in a keystone member of the gut microbiota. Cell Host Microbe. 2022 Feb 9;30(2):183-199.e10.

37. Tawk C, Lim B, Bencivenga-Barry NA, Lees HJ, Ramos RJF, Cross J, et al. Infection leaves a genetic and functional mark on the gut population of a commensal bacterium. Cell Host Microbe. 2023 May 10;31(5):811-826.e6.

38. Sakamoto A, Terui Y, Yoshida T, Yamamoto T, Suzuki H, Yamamoto K, et al. Three Members of Polyamine Modulon under Oxidative Stress Conditions: Two Transcription

Factors (SoxR and EmrR) and a Glutathione Synthetic Enzyme (GshA). PLoS ONE. 2015 Apr 21;10(4):e0124883.

39. Tian T, Wang Z, Zhang J. Pathomechanisms of Oxidative Stress in Inflammatory Bowel Disease and Potential Antioxidant Therapies. Oxid Med Cell Longev. 2017;2017:4535194.

40. Pasternak BA, D'Mello S, Jurickova II, Han X, Willson T, Flick L, et al. Lipopolysaccharide exposure is linked to activation of the acute phase response and growth failure in pediatric Crohn's disease and murine colitis. Inflamm Bowel Dis. 2010;16(5):856–69.

41. Jagt JZ, Struys EA, Ayada I, Bakkali A, Jansen EEW, Claesen J, et al. Fecal Amino Acid Analysis in Newly Diagnosed Pediatric Inflammatory Bowel Disease: A Multicenter Case-Control Study. Inflamm Bowel Dis. 2022 May 4;28(5):755–63.

42. Stacy A, Andrade-Oliveira V, McCulloch JA, Hild B, Oh JH, Perez-Chaparro PJ, et al. Infection trains the host for microbiota-enhanced resistance to pathogens. Cell. 2021 Feb 4;184(3):615-627.e17.

43. Son M, Ko JI, Kim WB, Kang HK, Kim BK. Taurine can ameliorate inflammatory bowel disease in rats. Adv Exp Med Biol. 1998;442:291–8.

44. Buret AG, Allain T, Motta JP, Wallace JL. Effects of Hydrogen Sulfide on the Microbiome: From Toxicity to Therapy. Antioxid Redox Signal. 2022 Feb 1;36(4–6):211–9.

45. Maeda T, Wakasawa T, Shima Y, Tsuboi I, Aizawa S, Tamai I. Role of polyamines derived from arginine in differentiation and proliferation of human blood cells. Biol Pharm Bull. 2006 Feb;29(2):234–9.

46. Revilla-Nuin B, Reglero A, Martínez-Blanco H, Bravo IG, Ferrero MA, Rodríguez-Aparicio LB. Transport of N-acetyl-D-mannosamine and N-acetyl-D-glucosamine in Escherichia coli K1: effect on capsular polysialic acid production. FEBS Lett. 2002 Jan 30;511(1–3):97–101.

47. Freland L, Beaulieu JM. Inhibition of GSK3 by lithium, from single molecules to signaling networks. Front Mol Neurosci. 2012 Feb 20;5:14.

48. Inaba K, Kuroda T, Shimamoto T, Kayahara T, Tsuda M, Tsuchiya T. Lithium toxicity and Na+(Li+)/H+ antiporter in Escherichia coli. Biol Pharm Bull. 1994 Mar;17(3):395–8.

49. Chen CC, Tsuchiya T, Yamane Y, Wood JM, Wilson TH. Na+ (Li+)-proline cotransport in Escherichia coli. J Membr Biol. 1985;84(2):157–64.

50. Gatenby RA, Brown JS. Integrating evolutionary dynamics into cancer therapy. Nat Rev Clin Oncol. 2020 Nov;17(11):675–86.

51. Cai Z, Wang S, Li J. Treatment of Inflammatory Bowel Disease: A Comprehensive Review. Front Med. 2021 Dec 20;8:765474.

52. Öhman L, Lasson A, Strömbeck A, Isaksson S, Hesselmar M, Simrén M, et al. Fecal microbiota dynamics during disease activity and remission in newly diagnosed and established ulcerative colitis. Sci Rep. 2021 Apr 21;11(1):8641.

53. Kim SC, Tonkonogy SL, Albright CA, Tsang J, Balish EJ, Braun J, et al. Variable phenotypes of enterocolitis in interleukin 10-deficient mice monoassociated with two different commensal bacteria. Gastroenterology. 2005 Apr;128(4):891–906.

54. Moolenbeek C, Ruitenberg EJ. The “Swiss roll”: a simple technique for histological studies of the rodent intestine. Lab Anim. 1981 Jan;15(1):57–9.

55. Adolph TE, Tomczak MF, Niederreiter L, Ko HJ, Böck J, Martinez-Naves E, et al. Paneth cells as a site of origin for intestinal inflammation. Nature. 2013 Nov 14;503(7475):272–6.

56. Martin M. Cutadapt removes adapter sequences from high-throughput sequencing reads. EMBnet.journal. 2011 May 2;17(1):10.

57. Bolger AM, Lohse M, Usadel B. Trimmomatic: a flexible trimmer for Illumina sequence data. Bioinformatics. 2014 Aug 1;30(15):2114–20.

58. KneadData – The Huttenhower Lab [Internet]. [cited 2023 Jul 25]. Available from: https://huttenhower.sph.harvard.edu/kneaddata/

59. Deatherage DE, Barrick JE. Identification of Mutations in Laboratory-Evolved Microbes from Next-Generation Sequencing Data Using breseq. In: Sun L, Shou W, editors. Engineering and Analyzing Multicellular Systems [Internet]. New York, NY: Springer New York; 2014 [cited 2022 Oct 17]. p. 165–88. (Methods in Molecular Biology; vol. 1151). Available from: http://link.springer.com/10.1007/978-1-4939-0554-6_12

60. Kitamoto S, Alteri CJ, Rodrigues M, Nagao-Kitamoto H, Sugihara K, Himpsl SD, et al. Dietary L-serine confers a competitive fitness advantage to Enterobacteriaceae in the inflamed gut. Nat Microbiol. 2020 Jan;5(1):116–25.

61. Haslauer KE, Schmitt-Kopplin P, Heinzmann SS. Data Processing Optimization in Untargeted Metabolomics of Urine Using Voigt Lineshape Model Non-Linear Regression Analysis. Metabolites. 2021 Apr 29;11(5):285.

62. Dieterle F, Ross A, Schlotterbeck G, Senn H. Probabilistic Quotient Normalization as Robust Method to Account for Dilution of Complex Biological Mixtures. Application in 1H NMR Metabonomics. Anal Chem. 2006 Jul 1;78(13):4281–90.

63. Heinzmann SS, Waldenberger M, Peters A, Schmitt-Kopplin P. Cluster Analysis Statistical Spectroscopy for the Identification of Metabolites in 1H NMR Metabolomics. Metabolites. 2022 Oct;12(10):992.

64. Csárdi G, Nepusz T. The igraph software package for complex network research. In 2006 [cited 2023 Aug 11]. Available from: https://www.semanticscholar.org/paper/The-

igraph-software-package-for-complex-network-Cs%C3%A1rdi-Nepusz/1d2744b83519657f5f2610698a8ddd177ced4f5c

65. R: A Language and Environment for Statistical Computing | BibSonomy [Internet]. [cited 2023 Jul 27]. Available from: https://www.bibsonomy.org/bibtex/7469ffee3b07f9167cf47e7555041ee7

66. Faust K, Croes D, van Helden J. Metabolic pathfinding using RPAIR annotation. J Mol Biol. 2009 May 1;388(2):390–414.

67. Anderson MJ. A new method for non-parametric multivariate analysis of variance. Austral Ecol. 2001;26(1):32–46.

68. Bray JR, Curtis JT. An Ordination of the Upland Forest Communities of Southern Wisconsin. Ecol Monogr. 1957;27(4):325–49.

69. Rohart F, Gautier B, Singh A, Cao KAL. mixOmics: an R package for ‘omics feature selection and multiple data integration [Internet]. bioRxiv; 2017 [cited 2023 Jul 6]. p. 108597. Available from: https://www.biorxiv.org/content/10.1101/108597v1

70. Signorell A, Aho K, Alfons A, Anderegg N, Aragon T, Arachchige C, et al. DescTools: Tools for Descriptive Statistics [Internet]. 2023 [cited 2023 Jul 27]. Available from: https://cran.r-project.org/web/packages/DescTools/index.html